**JOURNAL OF CRITICAL REVIEWS**

ISSN- 2394-5125 VOL 07, ISSUE 19, 2020

# SYNTHESIS AND CHARACTERIZATION OF COPPER OXIDE NANOPARTICLES (CuO NPs) , THEIR BIOLOGICAL ACTIVITY AND AS A CONTRAST AGENT FOR ULTRASOUND IMAGING

**Sumit Yadav**
Research Scholar, Jayoti Vidyapeeth Women's University
Vedaant Gyan Valley, Village-Jharna, Mahala, Jobner Link Road, NH-08,
Jaipur Ajmer Express Way, Jaipur (Rajasthan) India
yadav.sumit974@gmail.com
**Dr. Sourabh Jain**
Research Guide, Jayoti Vidyapeeth Women's University
Vedaant Gyan Valley, Village-Jharna, Mahala, Jobner Link Road, NH-08,
Jaipur Ajmer Express Way, Jaipur (Rajasthan) India
research@jvwu.ac.in
**Dr. Veenu Sisodia**
CNER, University of Rajasthan, Jaipur
drveenusisodia@gmail.com

## ABSTRACT
Due to its unique properties, such as being anti-fungal, antibacterial, and anti-rust, copper oxide nanoparticles (CuO NPs) play a significant role in a number of sectors today, including medicine, fertiliser, textiles, and clothing. We use an ecologically acceptable wet chemical process to create copper oxide nanoparticles (CuO NPs). CuO nanoparticle production (CuO NPs) was confirmed using a number of spectroscopic and microscopic analyses as well as other scientific tools. The materials were examined using X-ray diffraction (XRD), scanning electron microscopy (SEM), transmission electron microscope (TEM), Fourier change infrared (FTIR) spectroscopy, and voltage-current (V-I) BY Fourth probe technique. We also research antifungal and antibacterial properties as well as their use as contrast agents in ultrasound imaging.

**Keywords: Copper Oxide Nanoparticles (CuO NPs), Anti-bacterial Activity, Antifungal activity, XRD, FTIR, SEM, TEM, UV, V-I,Bacillus Subtilis, Pseudomonas Aeruginosa, Candida, A.niger, Ultrasound Imaging.**

## 1 INTRODUCTION
Since each individual is unique, nanoscience is beneficial in many different businesses. For example, the pharmaceutical industry uses it to create a variety of distinct medications that target specific patients. Nanotechnology may be used to create components for nanoscale electronics. One of the most significant types of oxide nanoparticles is copper oxide. Therefore, it is used in

ISSN- 2394-5125 VOL 07, ISSUE 19, 2020

the pharmaceutical industry, the creation of Nano electrical devices, the manufacturing of pants, clothing, and textiles, and its utilisation in the biomedical field is undoubtedly non-toxic.

Here, copper oxide nanoparticles (CuO NPs) are synthesized and characterized, and various biological effects on various types of microorganism are observed. Because of their anti-fungal and anti-microbial properties, copper oxide nanoparticles are utilised in the food-processing industry and as a contrast agent in ultrasound imaging.

Copper oxide (CuO) is used in a wide range of industries, including electronics, sensors, environmental technology, and the conversion and storage of energy [1]. CuO nanoparticles are employed to increase the viscosity of fluids that transfer energy, which increases thermal conductivity [2]. Recent developments in the field of technology and science, particularly in nanotechnology, have led to the creation of a novel concept for generating nanoscale trash in desired sizes and shapes [3,4]. Compared to organic antibacterial agents, CuO nanoparticles are stable, robust, and have a longer shelf life [5-8]. Additionally, CuO nanoparticles were used as anti-microbial agents. [9-10]. The monoclinic form system includes copper oxide nanoparticles [11–14]. This metallic oxide is extensively employed in the creation of organic-inorganic nano composites [20], superconductors [15,16], gas sensors [17–19], and large magneto resistance materials [15,16]. Copper oxide nanoparticles have important roles in medicine as both antibacterial and antioxidant agents [21, 22]. They are also included in the formulations of pesticides [23]. They are used in the manufacturing process as thermal conductors [24], catalysts [25], batteries [26], solar cells [27], and contrast agents for ultrasound imaging.

## 2 COPPER OXIDE NANOPARTICLES (CuO NP) SYNTHESIS METHOD

We used a 0.2 M $\mathbf{Cu(NO_3)_2}$ solution and 0.4 M NaOH to create copper oxide nanoparticles using a wet chemical technique. Copper nitrates were dissolved in water before sodium hydroxide was gradually added while being stirred constantly at room temperature. Copper hydroxide was created in this.

At 83 degrees Celsius, the stirring continued constantly for 6.30 hours. Following the reaction, the liquid was filtered before being baked at 65 degrees Celsius to dry it out. We produced copper oxide nanoparticles from these hydroxides by calcining them at 610 degrees Celsius in a furnace (CuO NP). Different experimental tools, including X-ray diffraction (XRD), scanning electron microscopy (SEM), transmission electron microscopy (TEM), Fourier transform infrared (FTIR), and ultra-violet spectroscopy, were used to describe this product (UV). Current and voltage characteristics using the fourth probe technique (V-I).

## 3 XRD ANALYSIS –WE DISCUSSED X-RAY DIFFRACTION OF OUR CuO NP-

To look for the crystallinity and particle characteristics typical of synthetic nanoparticles, X-ray diffraction experiments were performed on synthesized particles. The XRD design of copper oxide nanoparticles is shown by the after numbers. Peaks for CuO NPs generated sheep appear at this time to be utilizing matter, $2\theta = 33.1°$ (110), 35.41° (002), 39.12° (111), 49.17° (202),

ISSN- 2394-5125 VOL 07, ISSUE 19, 2020

53.11° (020), 58.31° (202), 62.01° (113), 66.10° (311), 68.01° (113),73.11°(311),75.01°(004) respectively. By utilizing Debey-Scherrer equation

$$D = 0.9\lambda/\beta Cos\theta$$

where D, k, λ, and β represent the average crystal size, shape factor (0.9), wavelength (0.15416) and Bragg angle θ associated with the X-ray (1.5406 Å) Cu Ka radiation correspondingly. The average CuO NPs crystallite size was determined as 360.70 nm.

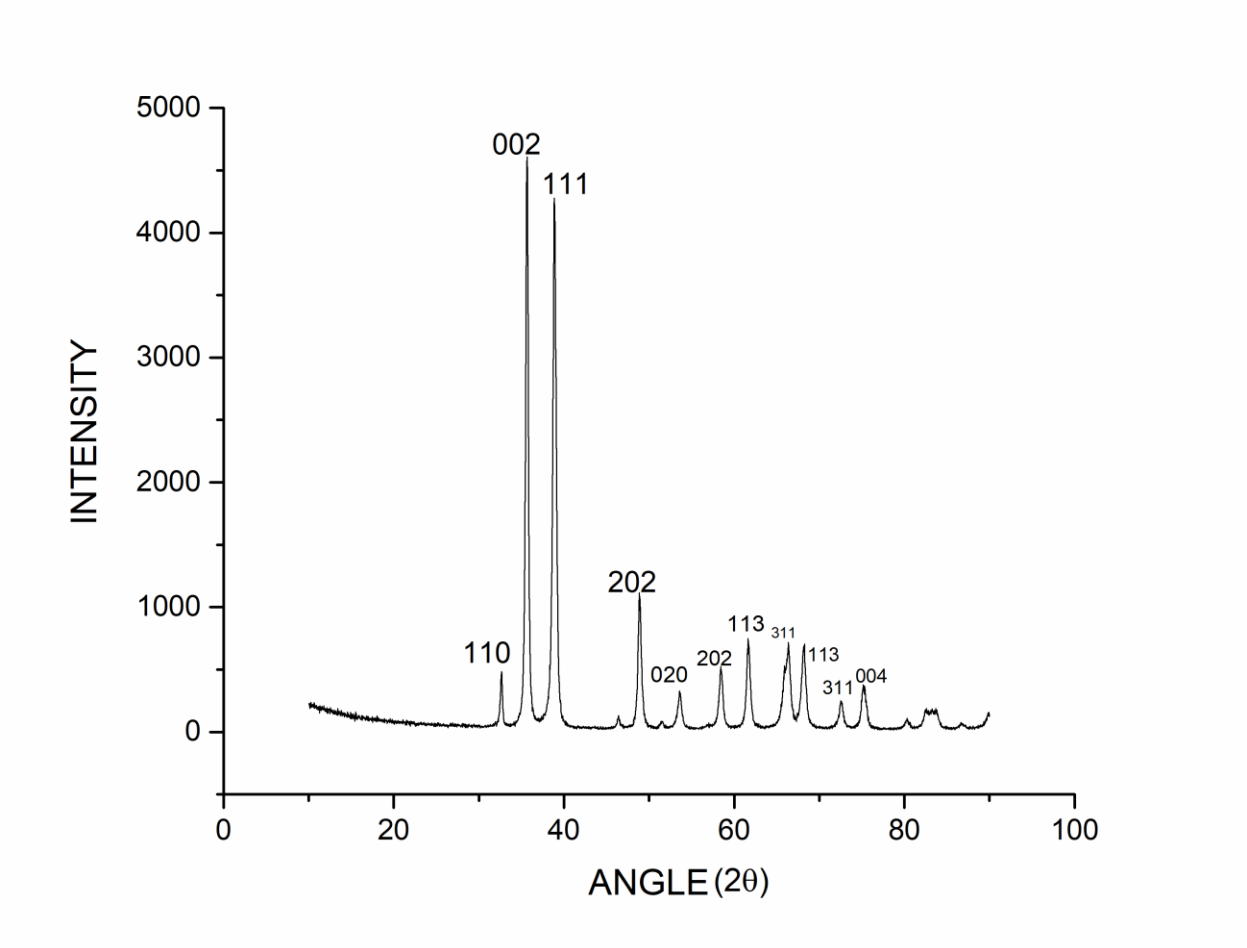


## 4 SCANNING ELECTRON MICROSCOPE (SEM) ANALYSIS-

The morphology associated with the NPs that is synthesized analyzed by scanning electron microscopy. The average particle size 0.3321µm, 0.4928µm, 2.9508µm, 0.3242 µm and 1.0294µm from Fig. (a),(b) ,(c),(d),(e) respectively .shows the outer lining morphology associated with CuO NPs.

ISSN- 2394-5125 VOL 07, ISSUE 19, 2020

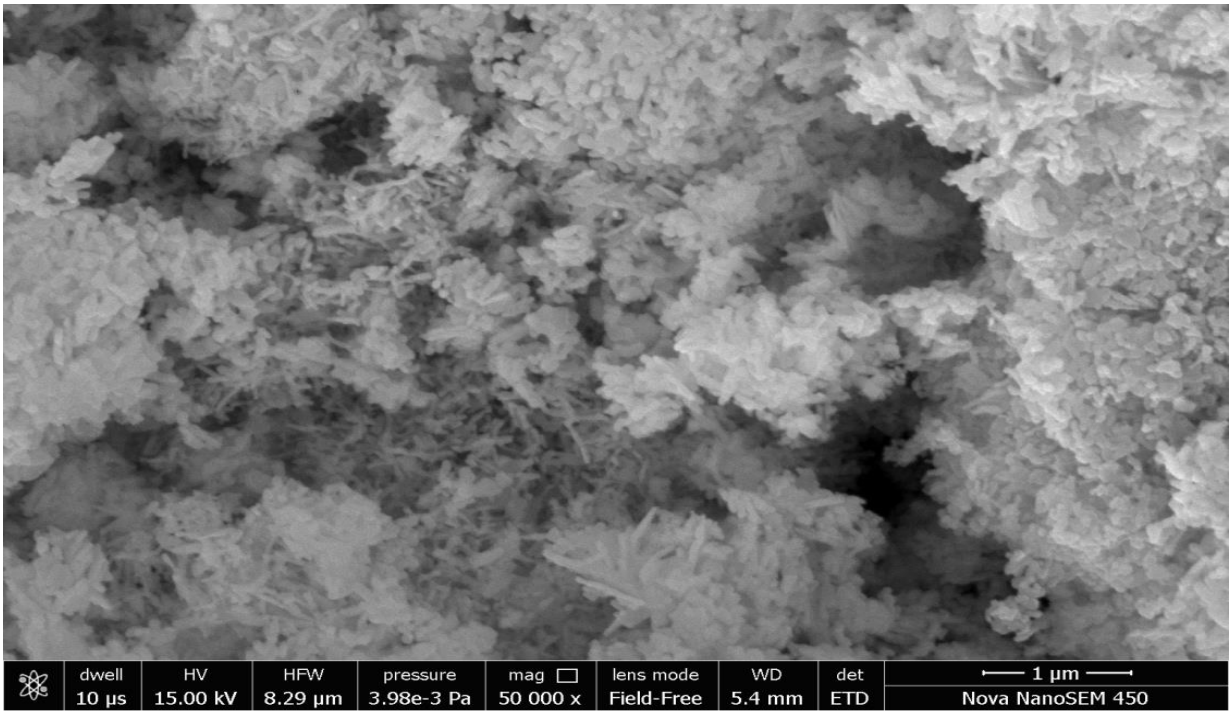


FIGURE-(a)

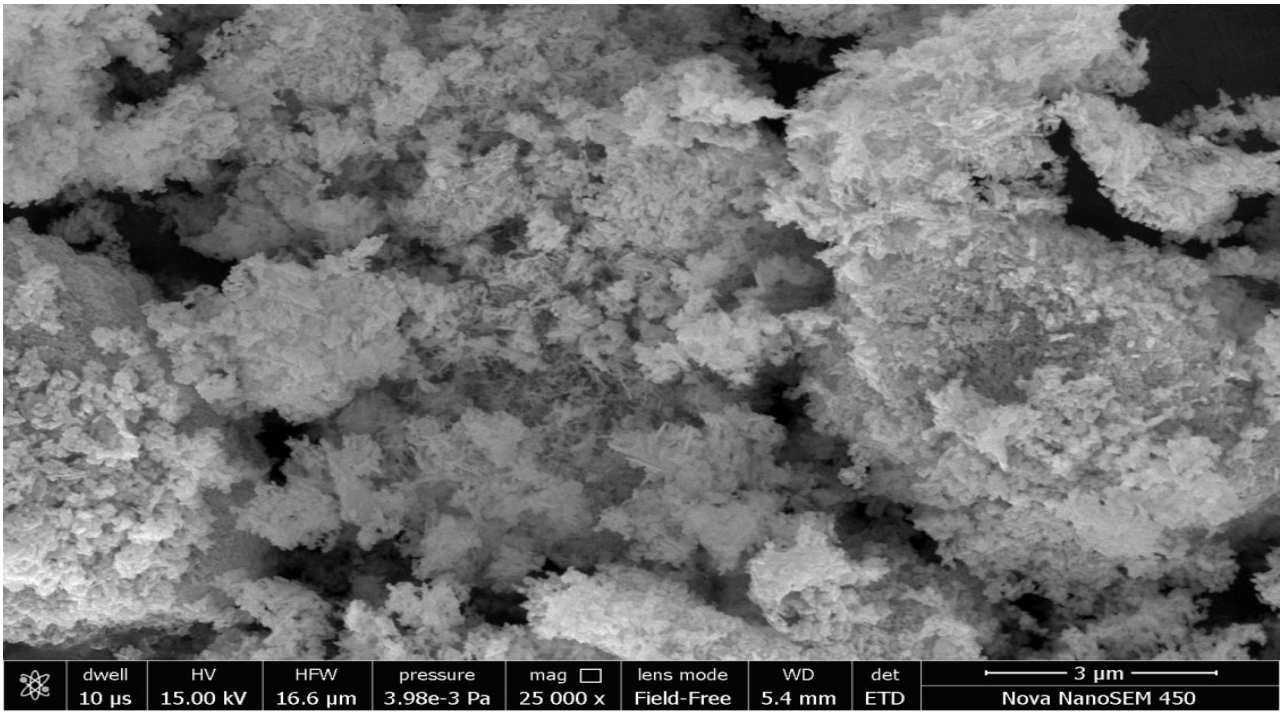


FIGURE-(b)

ISSN- 2394-5125 VOL 07, ISSUE 19, 2020

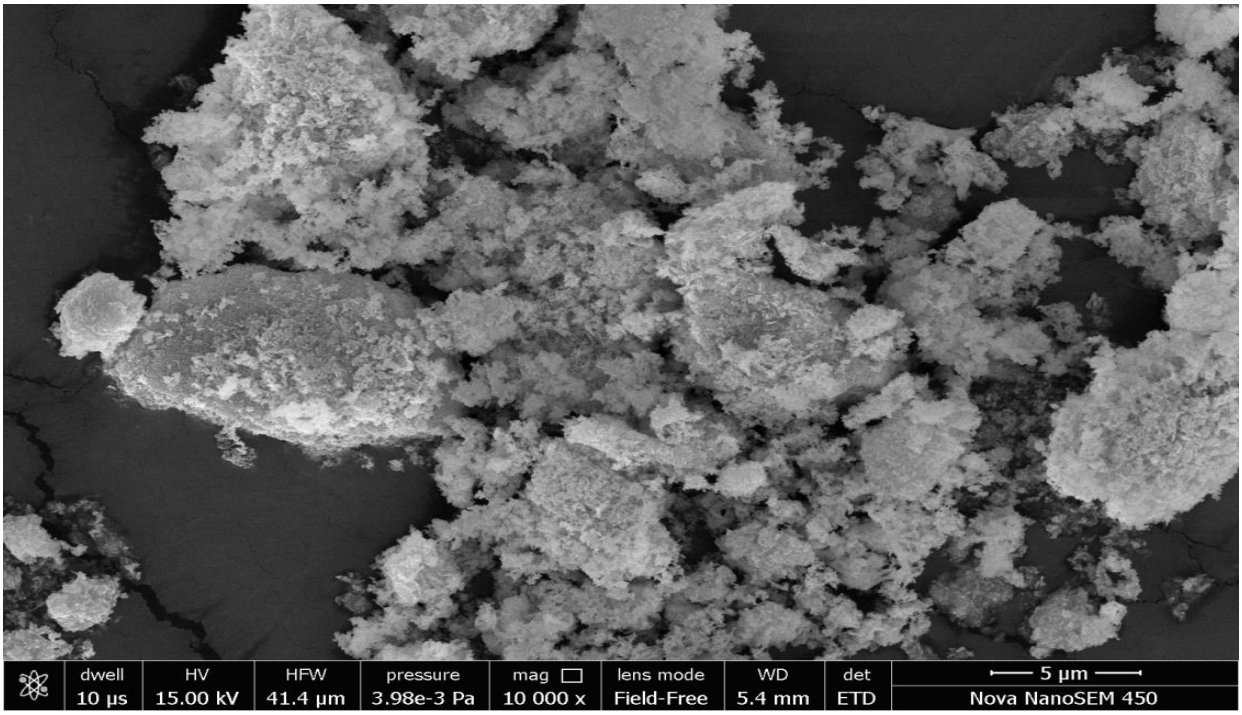


FIGURE-(c)

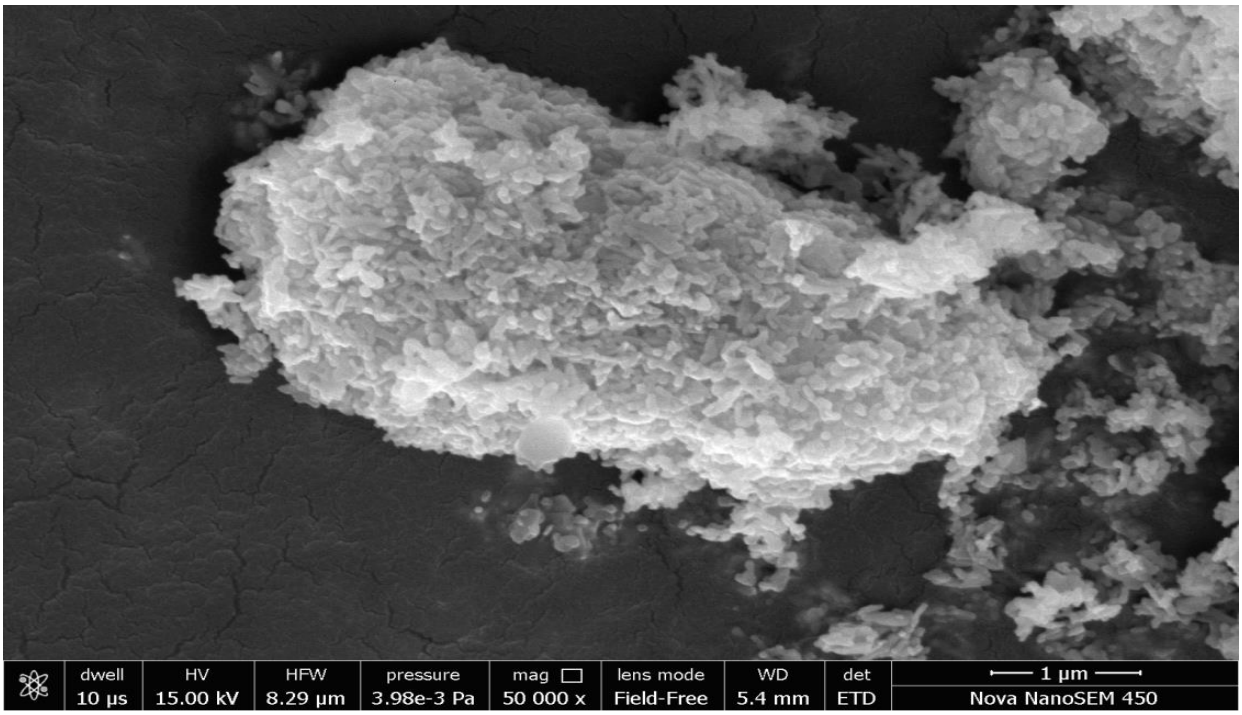


FIGURE-(d)

ISSN- 2394-5125 VOL 07, ISSUE 19, 2020

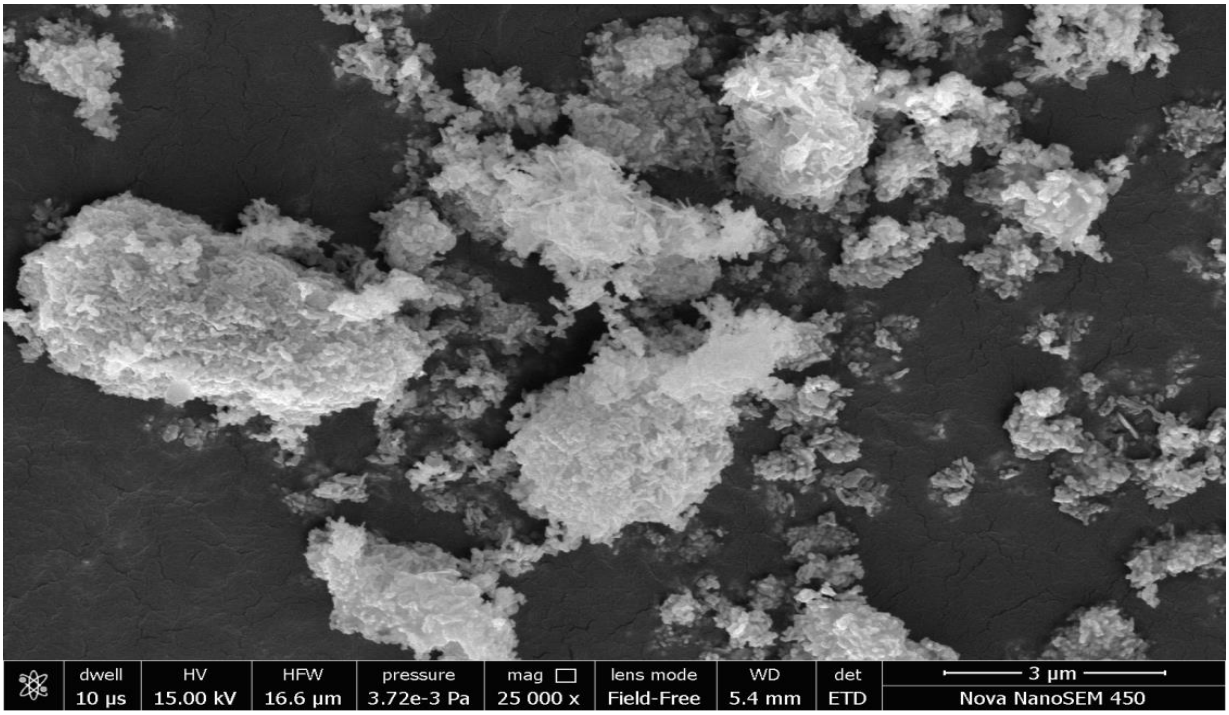


FIGURE-(e)

## 5 EDX (ENERGY DISPERSIVE X-RAY ANALYSIS)-

From SEM EDX we get the information percentage of elements present in Sample.

- The Energy dispersive X-ray analysis (EDX) pattern confirmed that the CuO nanoparticles were successfully conformed using the wet chemical technique.
- The locations of the EDX peak corresponded to copper and oxide.
- The crystalline structure of the produced CuO nanoparticles was shown by the EDX's strong peaks. The accompanying products were predominantly crystalline in character, according to the energy dispersive X-ray analysis and all the readings shown in the table below. This is shown by the high intensity and restricted range of CuO diffraction peaks.
- Using EDX analysis, the highest percentages of copper (Cu) and oxide (O) peaks were confirmed.
- The EDX examination showed the nanoparticles' chemical make-up, which had minuscule percentages of 79.20 for copper and 20.80 for oxygen.
- It was determined by EDX analysis that there was no critical contamination in the synthetic material. We can observe that there are pure crystalline copper oxide nanoparticles present.

ISSN- 2394-5125 VOL 07, ISSUE 19, 2020

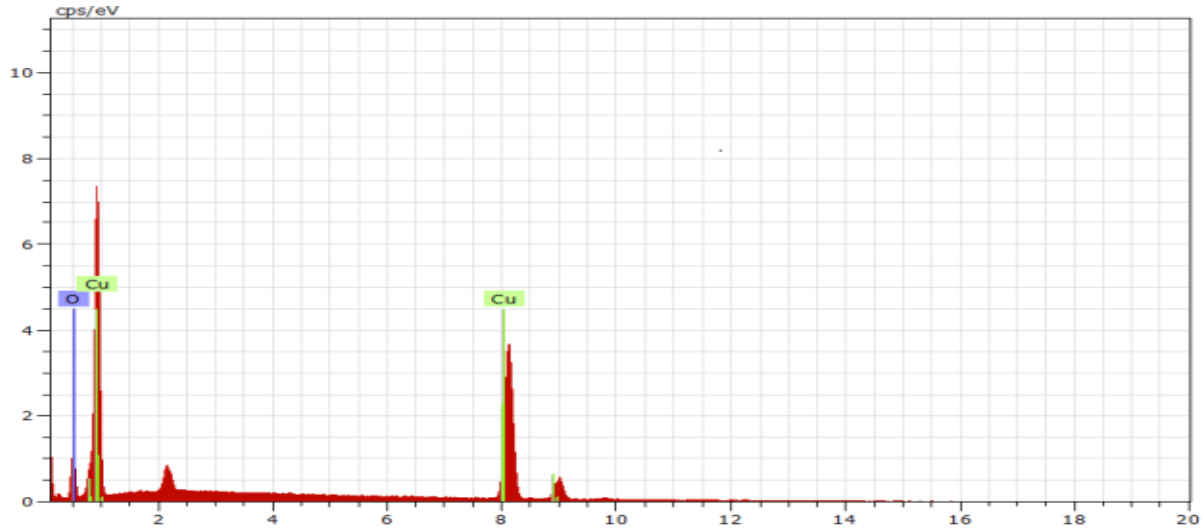


FIGURE-(f)

SPECTRUM: Acquisition 574

| EL | AN | SERIES | Unn. (Wt.%) | C norm (wt.%) | C atom (wt.%) | C Error (1 sigma) (wt.%) |
|---|---|---|---|---|---|---|
| Cu | 29 | K-series | 68.89 | 93.80 | 79.20 | 1.99 |
| O | 8 | K-series | 4.56 | 6.20 | 20.80 | 0.75 |
| | | Total : | 73.44 | 100.00 | 100.00 | |

## 6 TRANSMISSION ELECTRON MICROSCOPY (TEM) –

The size of produced nanoparticles, according to TEM images, is in the nanometer range. The sizes and structural morphologies of CuO-NPs were observed using TEM imaging. As seen in Figures (a), (b), (c), (d), and (e), the shapes of the CuO-NPs tend to be spherical. a small concentration. The average particle sizes in figures (a), (b), (c), (d), and (e) are 56.77 nm, 59.48 nm, 65.18 nm, 58.09 nm, and 64.66 nm, which indicate the crystallite structure.

ISSN- 2394-5125 VOL 07, ISSUE 19, 2020

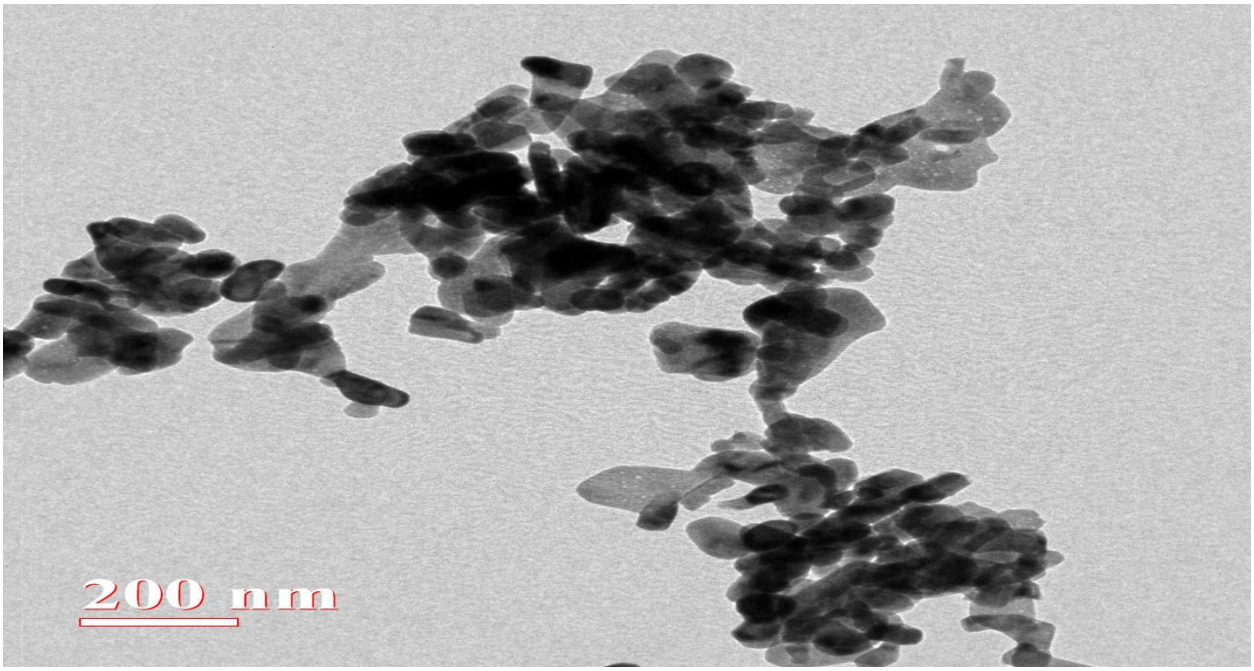


FIGURE-(a)

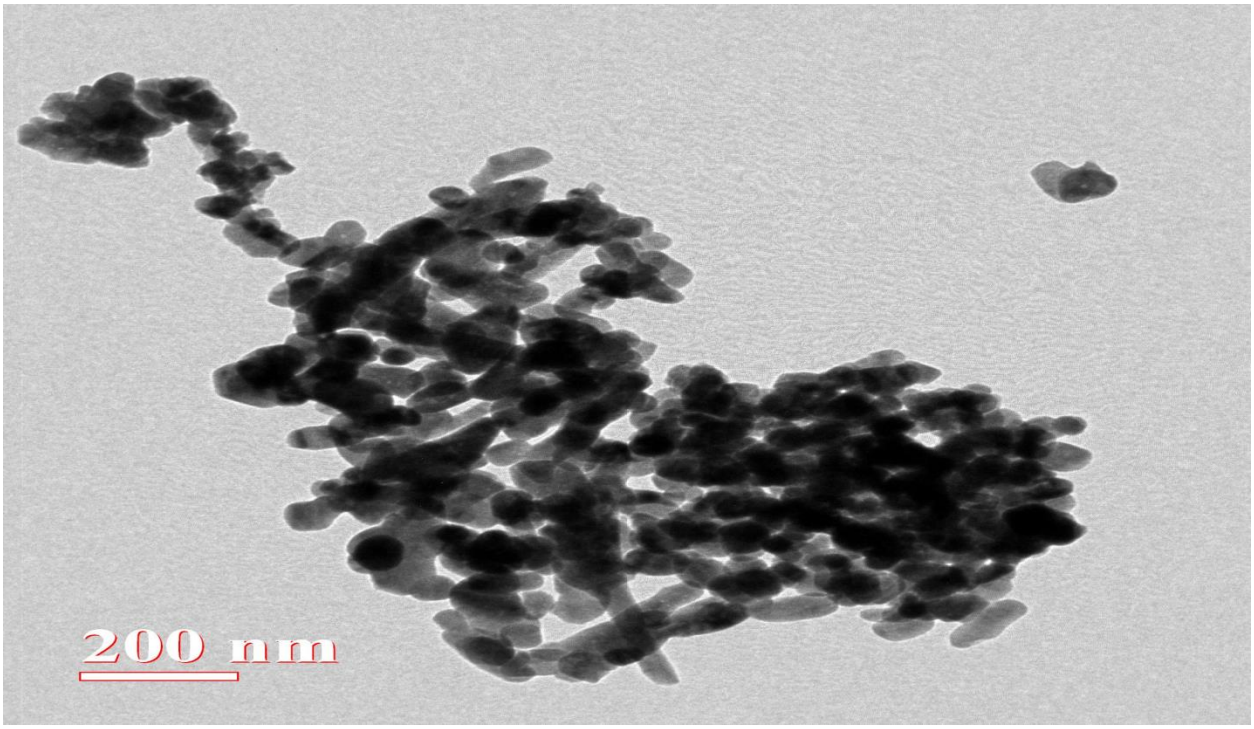


FIGURE-(b)

ISSN- 2394-5125 VOL 07, ISSUE 19, 2020

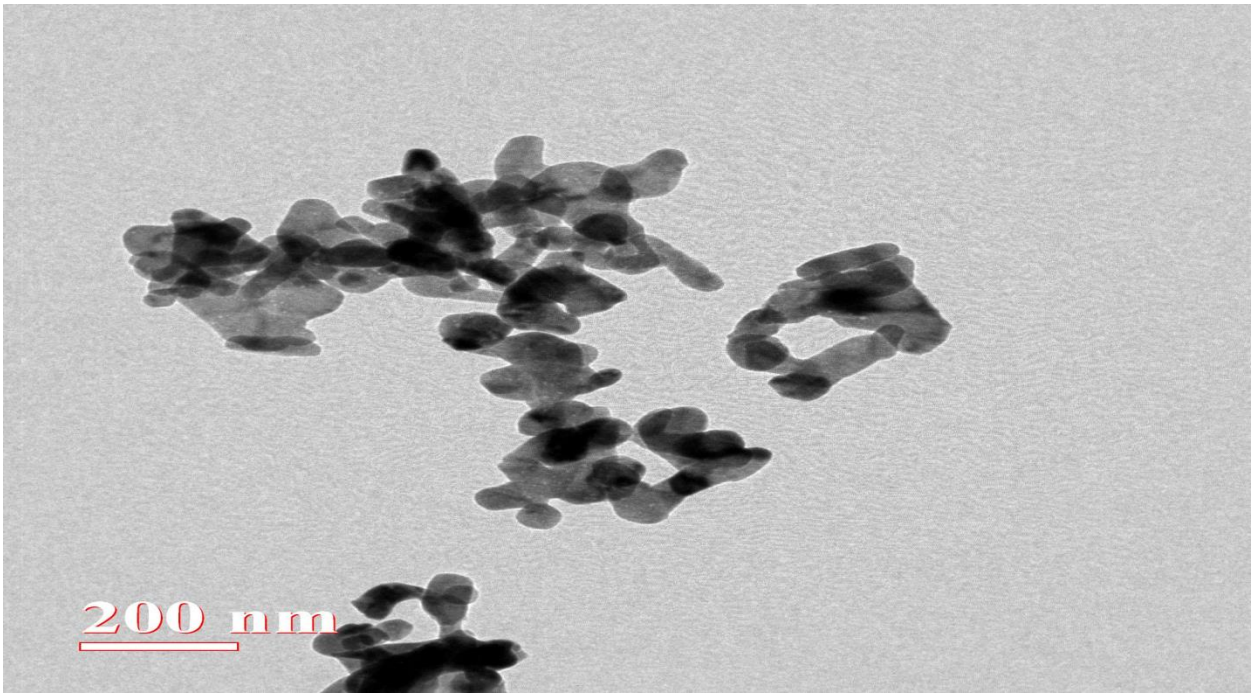


FIGURE-(c)

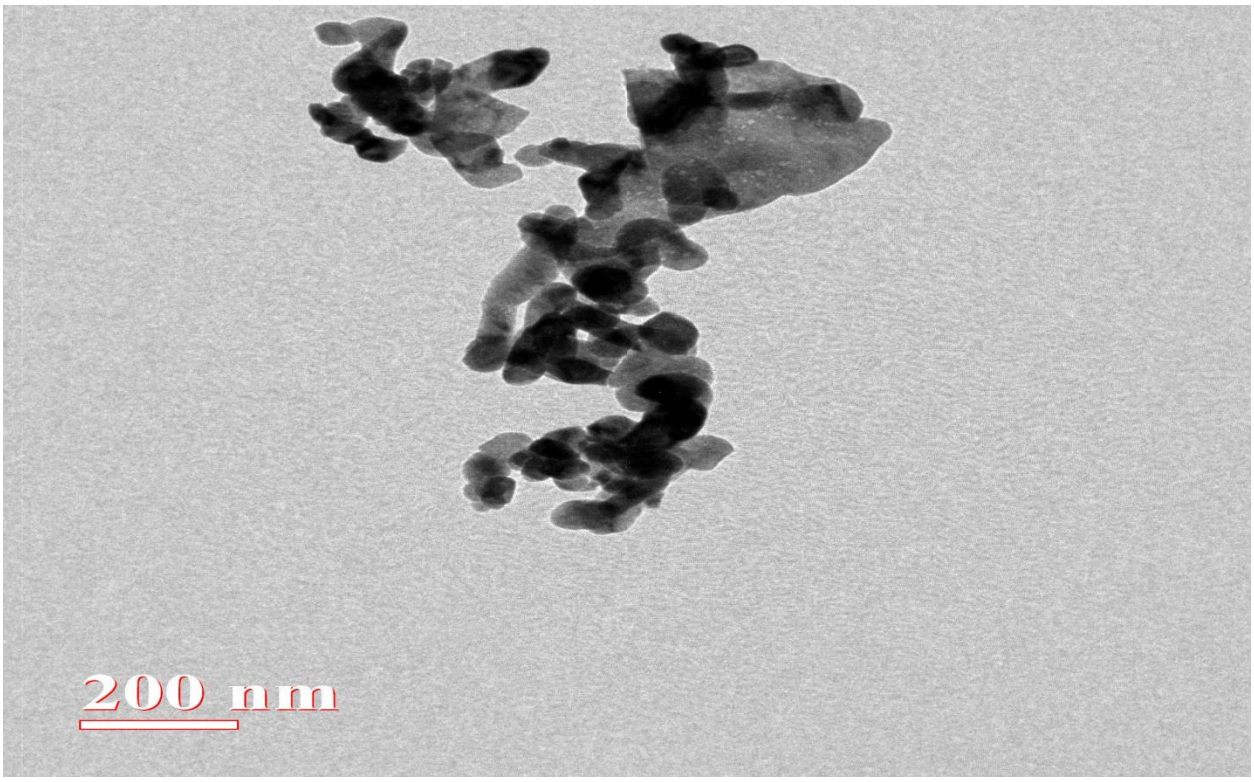


FIGURE-(d)

ISSN- 2394-5125 VOL 07, ISSUE 19, 2020

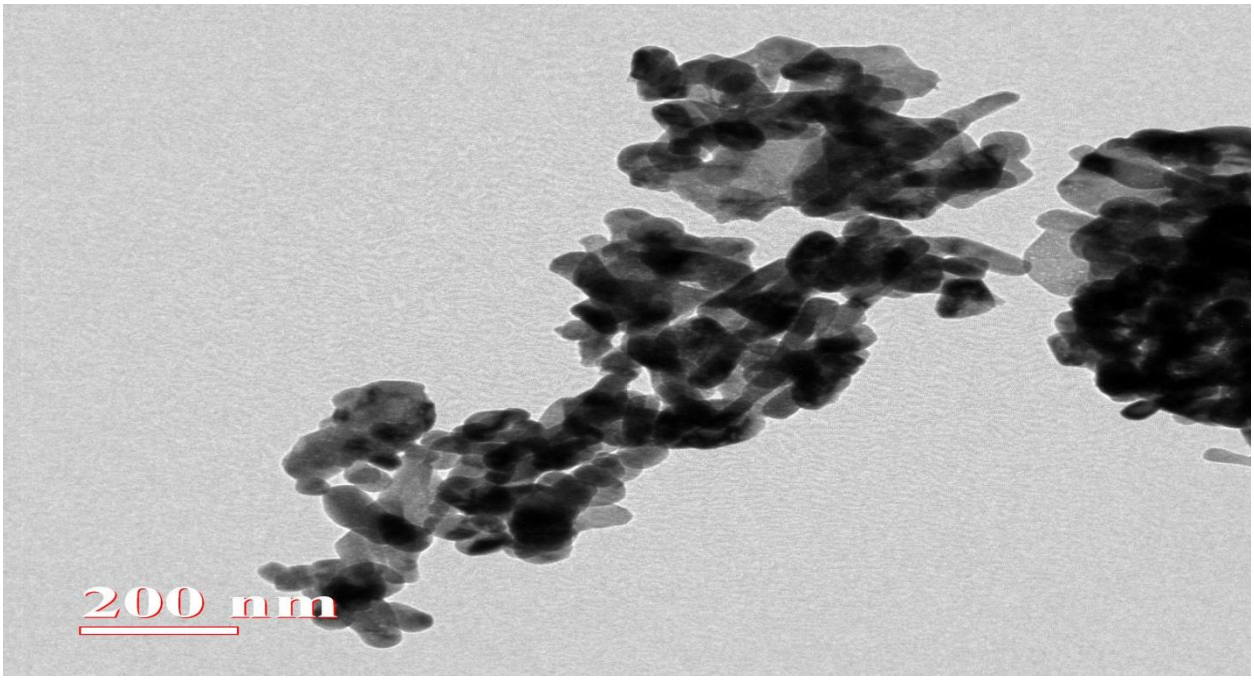


FIGURE-(e)

## 7 FOURIER TRANSFORM INFRA RED ANALYSIS-

The identification of functional groups in compounds may be done with the use of the characterization method known as Fourier transform infrared spectroscopy. The image below displays the FTIR spectra of CuO nanoparticles with a wavenumber range of 400 to 4000 cm-1. The top that is occurrence of band correlate to amide N-H stretching 3437.59 cm-1.

Alkane C-H stretches to its modest peaks at 2932.8 cm-1 and 2860.04 cm-1. Peaks at 1630.43 cm-1 originate from the bending of C=O anhydride

The method's 1384.04 C-N stretch peak is caused by the amine group, and its 1097.85 cm-1 C-O group peak. When looking at the CuO NPs Sample, the previously detected bands had been changed to 3437.59, 2932.8, 2860.4, 1630.43, 1384.04, 1097.85, 509.01, 505.97, and 444.73 (Cu-O band) cm1.

This F.T.I.R. graph shows peaks that were caused by several functional groups, which is quite helpful. Sharp, moderate, and weak peaks are often seen. There is a strong peak at 3437.59 cm-1, which may be the consequence of the amide N-H stretching.

ISSN- 2394-5125 VOL 07, ISSUE 19, 2020

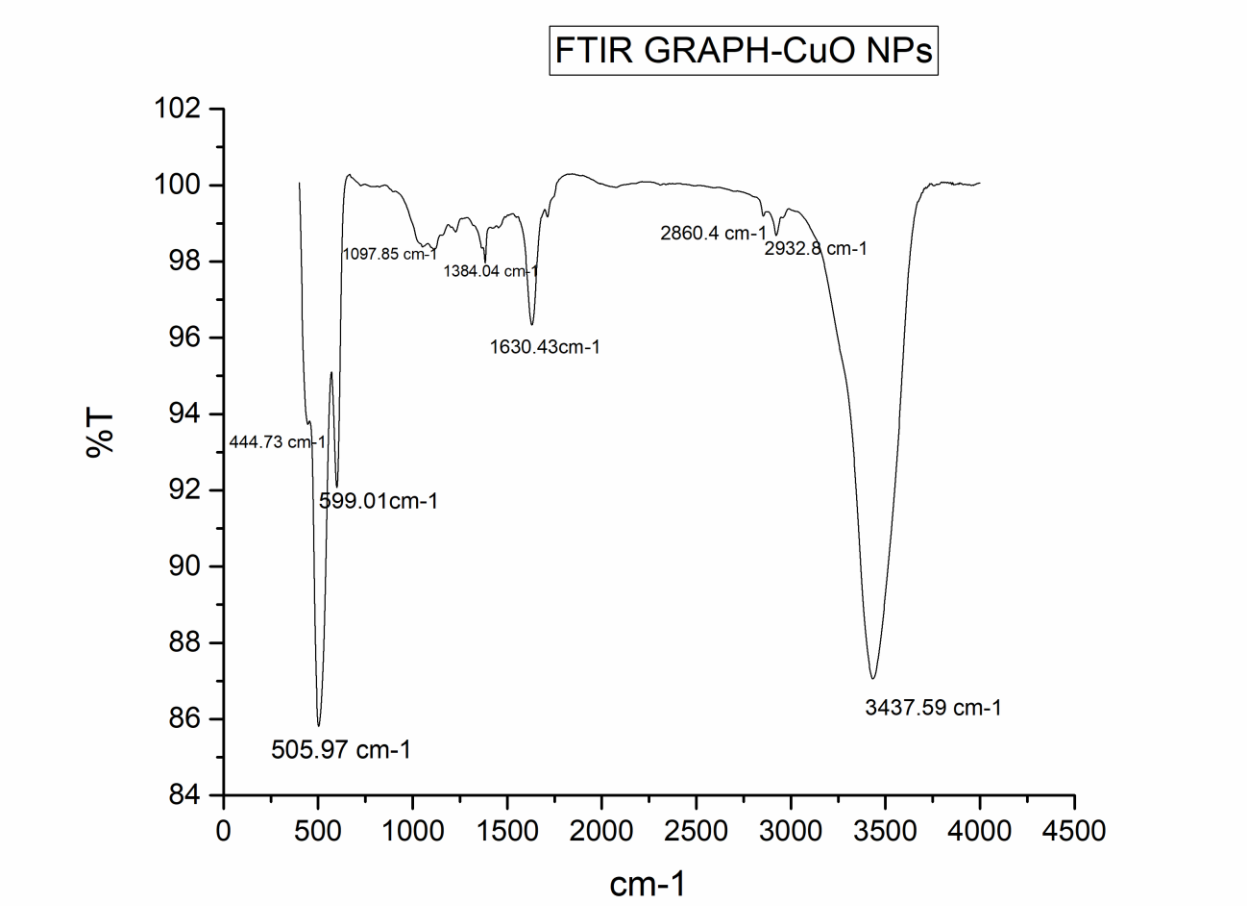


## 8 UV-Visible Spectroscopy

The characterization technique known as Fourier transform infrared spectroscopy may be used to identify functional groups in substances. The FTIR spectra of CuO nanoparticles with a wavenumber range of 400 to 4000 cm-1 are shown in the figure below. The band's top, which is amide N-H spanning 3437.59 cm-1, is an occurrence.

The minor peaks of alkane C-H are at 2932.8 cm-1 and 2860.04 cm-1. Peaks at 1630.43 cm-1 result from C=O anhydride bending.

The amine group and its 1097.85 cm-1 C-O group peak are responsible for the method's 1384.04 C-N stretch peak. The previously identified bands were now 3437.59, 2932.8, 2860.4, 1630.43, 1384.04, 1097.85, 509.01, 505.97, and 444.73 (Cu-O band) cm1 when looking at the CuO NPs Sample.

It is quite useful that this F.T.I.R. graph displays peaks that were brought on by various functional groups. Sharp, weak, and moderate peaks are often seen. A prominent peak can be seen at 3437.59 cm-1, which could be the result of amide N-H stretching.

ISSN- 2394-5125 VOL 07, ISSUE 19, 2020

Optical energy band gap associated with the CuO NPs was found becoming 3.3 ev, The Tauc's Equation is $(\alpha h\nu)^2 = A\ (h\nu\text{-}Eg)$

Where A is the proportionality constant and varies with the product, n is the index, and might be the absorption coefficient. H denotes the photon's energy. We appropriately draw the graph between h and (hv)2 on the X and Y axes. The band gap in this case will be 3.3 eV, as seen by the intercept on the x-axis.

In figure (B)

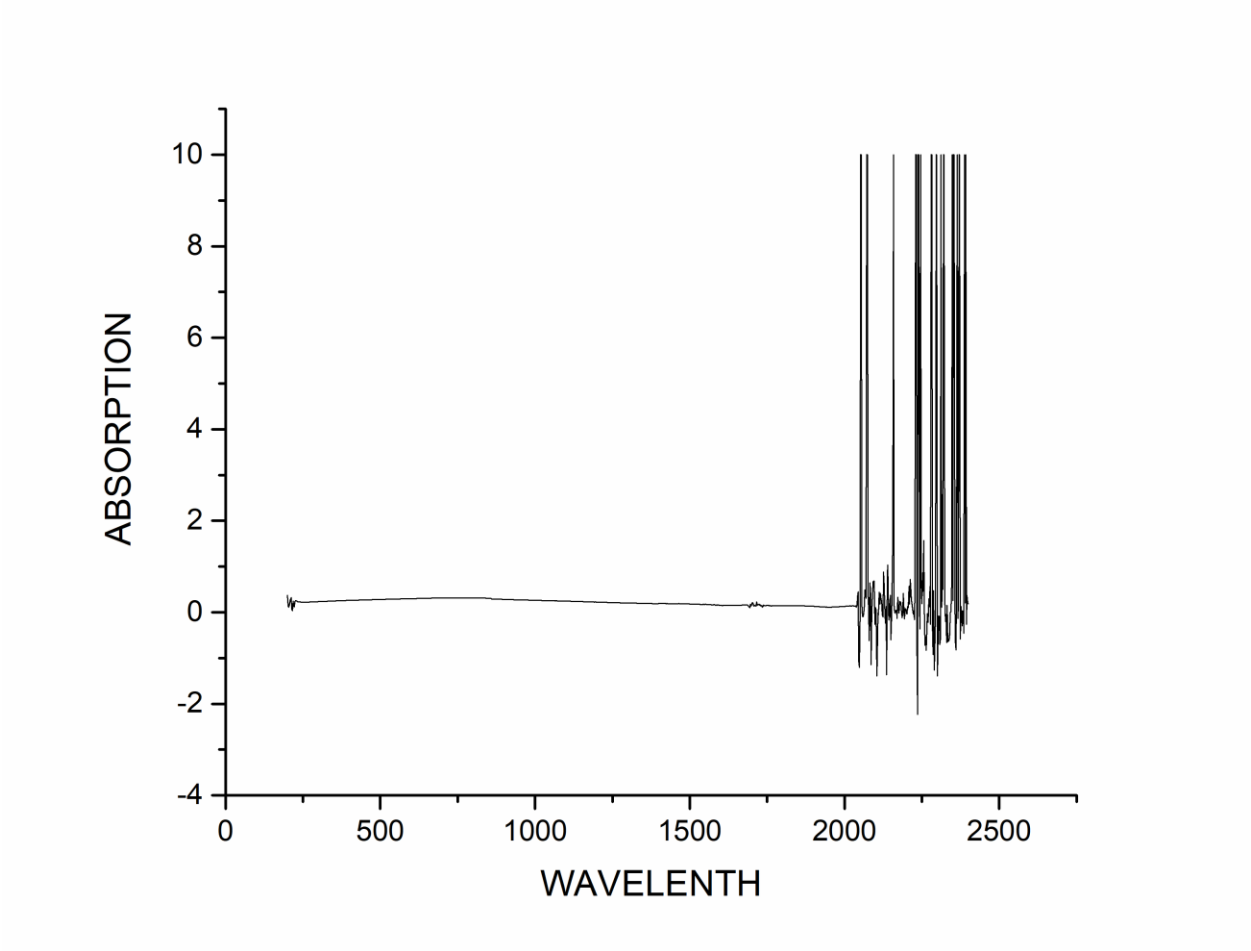


FIGURE-(A)

ISSN- 2394-5125 VOL 07, ISSUE 19, 2020

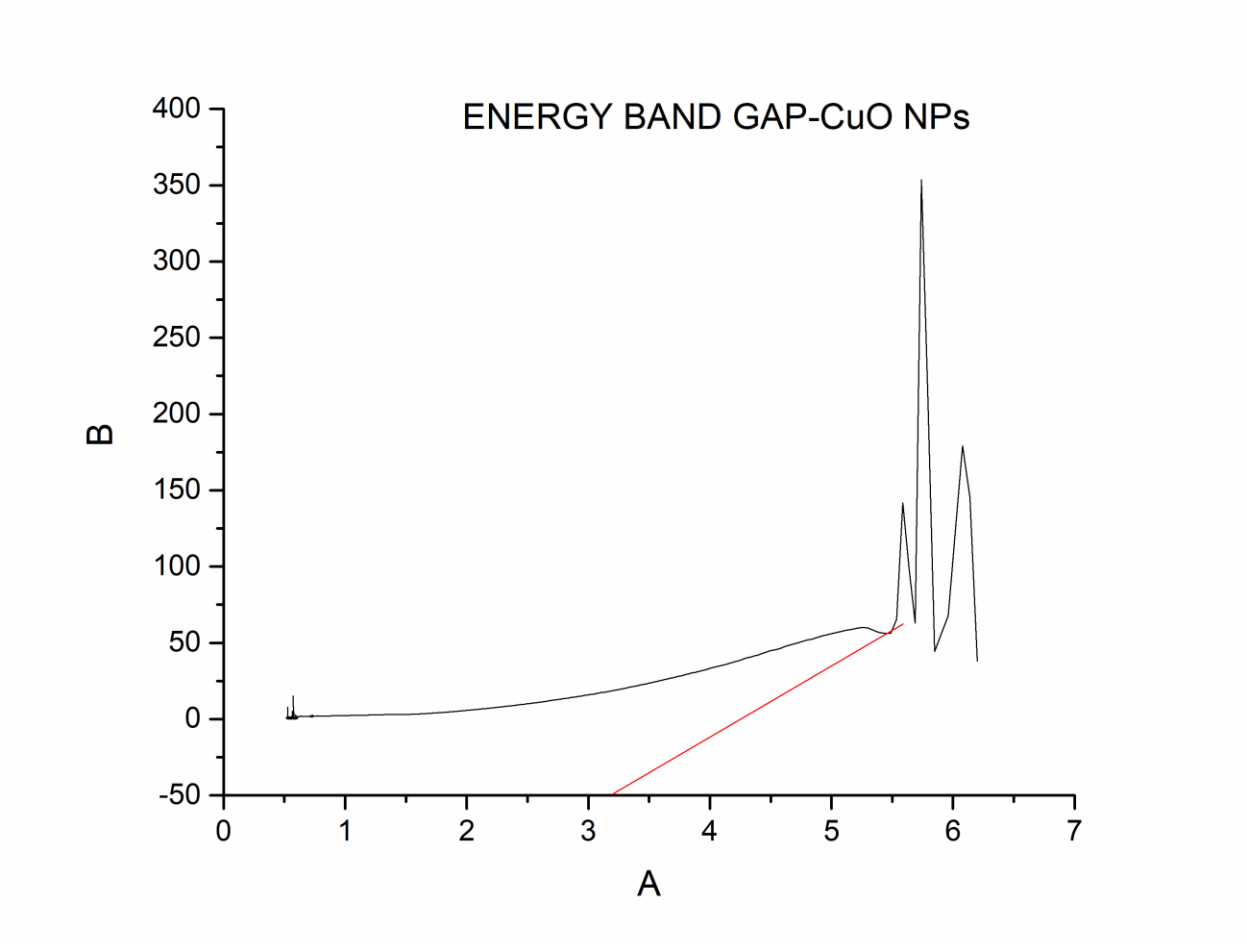


FIGURE-(B)

## 9 V-I (VOLTAGE PRESENT CHARECTERIZATION)

Physics study has been carried out for a product, which is monitoring the electric property of a material using a four-point probe technique. This research evaluates the present and the recent. The result may be used to calculate the material's resistivity. We make use of samples with a thickness of I called copper oxide nanoparticles. And there is a 1mm gap between each probe. Here, the sample's depth (t) is much less than the distance between probes (or (tS)). Here, we use a formula for determining the usual resistivity that is

RESISTIVITY ($\rho$) = $\pi$/log2( V/I)

After calculation the resistivity this is certainly average 26.07 X $10^9$ohm.meter

ISSN- 2394-5125 VOL 07, ISSUE 19, 2020

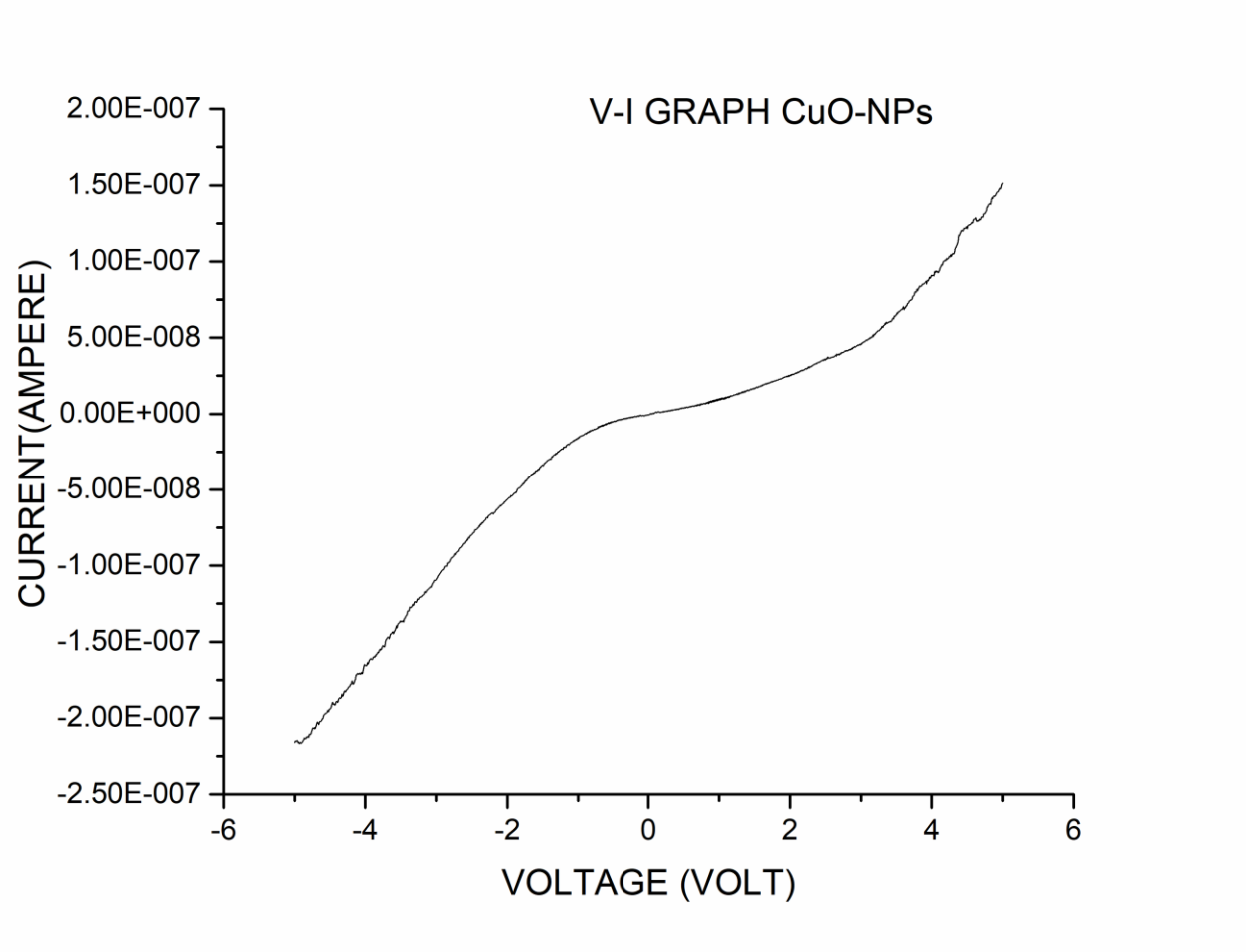


**Ultrasonic imaging with copper oxide nanoparticles**

CuO NPs have two acoustic characteristics that could be used as possible contrast sources in ultrasonic Both acoustic attenuation and speed of sound (SOS) in imaging were investigated. Measuring ultrasound sound speed.

Only deionized water was utilised for comparison, and the following concentrations of three solutions of 6 nm copper oxide NPs were examined: 42, 79, and 160 $g.mL^{-1}$. With an accuracy of +1 ns, an ultrasonic time of flight (TOF) gauge was connected to an 11MHz ultrasound transducer. The transducer was permanently fixed and operated in pulse-echo mode inside a 30 mL glass container. The solution's temperature was continuously monitored. The experiment's temperature (23.7 + 0.1 °C) was used to calculate the sound speed in water. (1488.2 $ms^{-1}$) [28] using standard relations. Three time-of-flight (TOF) measurements were then collected for each concentration. These observations demonstrate that the speed for the solutions under consideration was estimated.

**Measuring the ultrasonic attenuation coefficient**

Two ultrasonic transducers were mounted in alignment in a water tank. a 43 mL jar with two horizontal sides that is fastened and filled with clean water. A temperature sensor consisting of

ISSN- 2394-5125 VOL 07, ISSUE 19, 2020

fiber optics continuously recorded the temperature at 21.18 ± 0.04°C throughout the duration of the experiment. Utilizing the temperature that was observed and known relationships, the acoustic attenuation of water was calculated. CuO nanoparticle aliquots (0.1 mL of 4.317 mg/mL). They were then poured into distilled water together with a mixture of 6 nm-sized particles. A central frequency of 3.51MHz was obtained by 130 ultrasonic pulses utilizing a signal generator after stirring for 15 seconds and waiting 25 seconds after stirring. The signals were then amplified, band-pass filtered, and attenuated (350 KHz–30 MHz) after being received. A computer captured the signals after an analog-to-digital conversion (A/D) at 110MHz. The signal's envelope was then extracted using the Hilbert transform, and the acoustic attenuation of the investigated solution was calculated after that. The 130 attenuation coefficient values for each CuO concentration were then computed by averaging them and figuring out their standard deviation.

**An Experiment in Ultrasound through-transmission Imaging**

The presence of CuO NPs and their effect on acoustic attenuation through image transmission were used to assess the potential for improving image contrast. With this method, a target is scanned by sending an ultrasonic pulse from one side of the object and then detecting it on the other [29]. The amplitude of the transmitted waves is inversely associated with the integrated frequency. Attenuation along the wave's journey in terms of volume [30]. In our lab, a customized computer sonographic scanning system was developed [31]. Two focused transducers are placed side by side in a water tank. A 3D volume may be scanned using the system's computerized control interface. Signal transmission and detection were managed pulsar receivers using two computers. 45 J of pulse energy at 500 Hz PRF. The resultant waveform's effective Centre frequency is 3.51 MHz. A mechanical index (MI) of 0.35 was determined in respect to. Additional system parameters are available. In [33]. Two identical 55mL plastic tubes were filled with 15mL of deionized water and secured within the water tank. The tubes were scanned in raster mode along horizontal striations FOV = 74.1 X 24 $mm^2$ with vertical and horizontal resolutions of 0.3mm and 0.5mm. Analog band pass filtering was used after recording the raw ultrasonic signals (A-lines). They were processed into pictures for 2D acoustic projection by sampling them at 110 MHz between 350 KHz and 30 MHz using an analog-to-digital digitizer. There were a total of seven scans performed, as follows: two baseline scans and five further scans. Scans are performed after injecting 0.3 mL of 1.5 $mL^{-1}$ 6 nm thick CuO NPs in each tube, together with 0.4 mL of ordinary deionized water, into the left tube and the control tube on the right. All pictures were then normalised with respect to the water's amplitude from the reference image by dividing each pixel value by the measured amplitude of the water outside the tubes. Then, using the six scanned images of the initial baseline image, a set of subtraction images are created by eliminating each of the six photographs. Using a 5 x 5 pixel median filter, high-frequency noise was reduced. Each image's 100 pixels in the left tube were compared to an identical-sized ROI in the right tube in order to estimate CNR values. The results were then entered into the equation below.-

ISSN- 2394-5125 VOL 07, ISSUE 19, 2020

$$\text{Contrast to noise ratio (CNR)} \triangleq \frac{|\bar{I}_{CuO} - \bar{I}_{background}|}{\sqrt{\sigma^2_{Cuo} + \sigma^2_{background}}} \quad (1)$$

where $I_{CuO}$ is the average signal of the CuO region of interest (ROI), $I_{background}$ is the average signal of the background ROI (taken in the 0 μg · $mL^{-1}$ CuO test tube), $(\sigma\ CuO)^2$ is the standard deviations for the CuO ROI, and $(b_{ackground})^2$ is the standard deviations for the background ROI.s

The resulting 6 images of subtraction were then shown as a "morphology" overlaid with a "functional" (CuO-containing area) pseudo-color graphic (Similar to the display in PET/CT) Grey baseline image [32]. The two photos were combined thereafter so that pixels with low subtraction values (less than 1.3% of the amplitude of water) are transparent and pixels with high values are visible.

## 10 Analyzing ultrasound contrast

CuO NPs sound velocity as a function of concentration in an aqueous solution. Increased sound speed was caused by an increase in NPs concentration. The graphic below shows the connection between acoustic attenuation and CuO NP concentration. It is evident that the attenuation coefficient constantly rises linearly (t-test, p 0.01). CuO NPs are clearly present in the left tube, and the signal is inversely correlated with the NP concentration. CNR in The estimated values for the ensuing subtraction images were 0.29, 3.29, 3.67, 4.43, 6.02, and 6.65 for the corresponding concentrations of 0 (control), 74, 144, 207, 265, and 318 g/mL1.

FIGURE-(1)

FIGURE-2

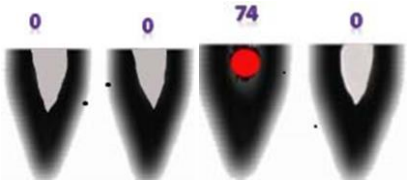

ISSN- 2394-5125 VOL 07, ISSUE 19, 2020

FIGURE-3

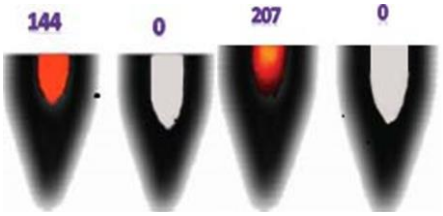


FIGURE-4

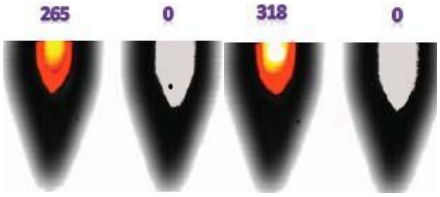


A baseline "morphology" picture is overlaid with a subtraction amplitude image from an ultrasonic through-transmission experiment (the amplitude image of the tubes without CuO). Figure-1 a photo of a 15 ml water tube that has been filled with water. Color. Figure 2-4 shows Overlay the subtraction pictures after 0.7 mL of 1.5 mg $mL^{-1}$ had been added. CuO is injected into the right tube and the left tube with 0.7 mL of deionized water (control). It's an integer. Above the tubes, a reading of the current CuO concentration (g/mL) is shown. It is clear that the CuO NPs generate a signal that is distinct and gets stronger with concentration.

**11 Antibacterial Task**

The agar well diffusion method was used to investigate the in vitro antibacterial efficacy of the test against gram-positive and gram-negative microbial strains (Perez et al., 1990). The Mueller Hinton agar No. 2 (Hi-Media, India) was used since this is a bacteriological approach. Dimethylsulphoxide (DMSO) was used to dilute the extracts at a concentration of 10 mg/mL. A standardised inoculum (1.5 108 CFU/mL, 0.5 McFarland) was then aseptically added to the molten Mueller Hinton agar and put onto sterile Petri dishes to produce a dish that is solid. The Mueller Hinton agar was then melted and chilled to 48–50°C. When you look at the agar that is definitely seeded, wells had been created. The test element was eventually added to the well in increments of 20, 40, 60, and 80 l. (6 mm). The dishes were incubated at 37°C overnight. The zone measurements surrounding each well were used to determine the range of antimicrobial herb for the microbiological species. The diameters of the region of inhibition produced by the broker were compared to those produced by the commercial control (Ciprofloxacin). To reduce error while still providing mean data, the experiment has been run three times.

ISSN- 2394-5125 VOL 07, ISSUE 19, 2020

The agar well diffusion technique was used to investigate the sample's in vitro antibacterial effectiveness against gram-positive and gram-negative microbial strains (Perez et al., 1990). When using the bacteriological approach, Mueller Hinton agar no. 2 (Hi-Media, India) was used. The extracts had been diluted in 10 mg/mL concentrations of 100% dimethyl sulphoxide (DMSO). A standardized inoculum (1.5 108 CFU/mL, 0.5 McFarland) was then aseptically added to the molten Mueller Hinton agar and placed onto sterile Petri dishes to produce a plate that is clearly solid. The Mueller Hinton agar was then melted and chilled to 48–50°C. In the seeded agar, wells were ready. In the end, the test chemical (20, 40, 60, and 80 l) was added to the well (6 mm). The dishes were incubated at 37°C overnight. The antibacterial spectrum of the herb was established in terms of bacterial species in terms of zone diameters surrounding each particle. The widths of the broker's zone of inhibition were different from those of the commercially available control (Ciprofloxacin). To lessen the mistake when the mean data were reported, the study was conducted three times. Bacteria are not impacted by copper oxide nanoparticles in any way.

## 12 Anti-bacterial Activity Against Bacillus subtilis

| TEST SAMPLE | STANDARD(CIPROFLOXACIN) | 20µI | 40µI | 60µI | 80µI |
|---|---|---|---|---|---|
| CuO | 39mm | NIL | NIL | NIL | NIL |

· Anti-bacterial Activity Against Pseudomonas aeruginosa

| TEST SAMPLE | STANDARD(CIPROFLOXACIN) | 20µI | 40µI | 60µI | 80µI |
|---|---|---|---|---|---|
| CuO | 37mm | NIL | NIL | NIL | NIL |

## 13 Determination of Antifungal Assay

Agar well diffusion technique is used to test the experimental anti-fungal activity of a plant (Bonjar et al, 2005). The fungal medium was Sabouraud's dextrose agar, SDA (Merck, Germany). Fungal spore suspensions were made in sterile PBS (phosphate buffer saline) and concentrated to a concentration of 106 cells per millilitre. At first look, this agar approach involves dipping a sterile brush into the fungus suspension system and rolling it. The seeded agar was made using wells. 20 to 80 l of the test chemical had been added to the well (6 mm). The dishes had undergone a 37°C incubation. Following a 24-hour incubation, bioactivities were dependent on the width of the inhibitory region (in mm). The representative's area of inhibition's diameters were compared to the controls' commercially produced diameters (ketoconazole).

ISSN- 2394-5125 VOL 07, ISSUE 19, 2020

Means were calculated for every experiment that had been performed in triplicate. Nanoscale copper oxide particles have antifungal properties.

**Antifungal Activity Against Candida**

| TEST SAMPLE | STANDARD (KETOCONAZOLE) | 20µl | 40µl | 60µl | 80µl |
|---|---|---|---|---|---|
| CuO | 30mm | 20mm | 24mm | 25mm | 26mm |

**Antifungal Activity AgainstA.niger**

| TEST SAMPLE | STANDARD (KETOCONAZOLE) | 20µl | 40µl | 60µl | 80µl |
|---|---|---|---|---|---|
| Cu0 | 23mm | 33mm | 34mm | 35mm | 36mm |

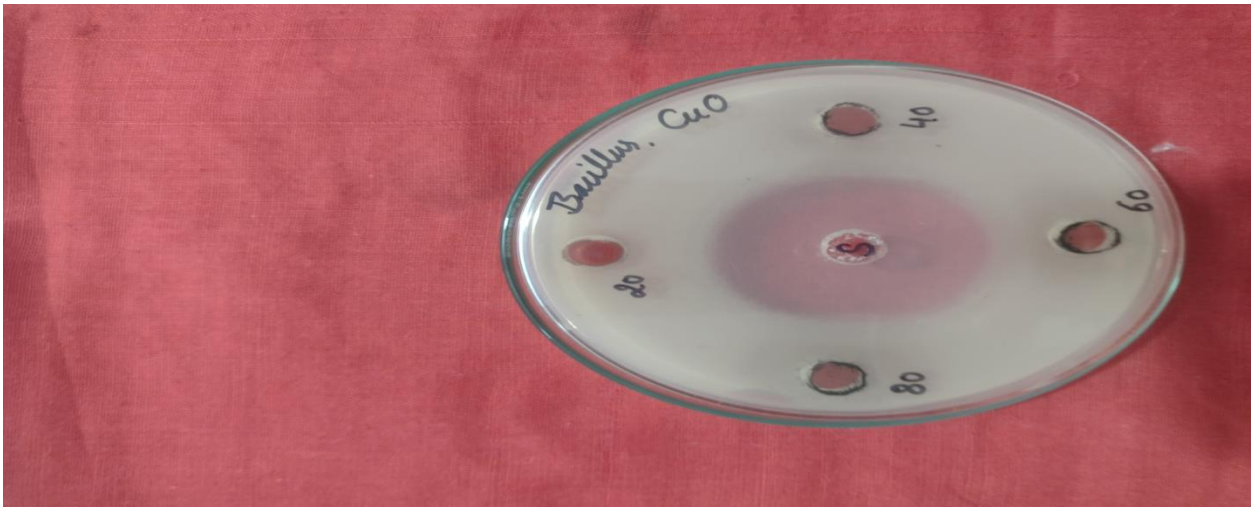


Figure-1

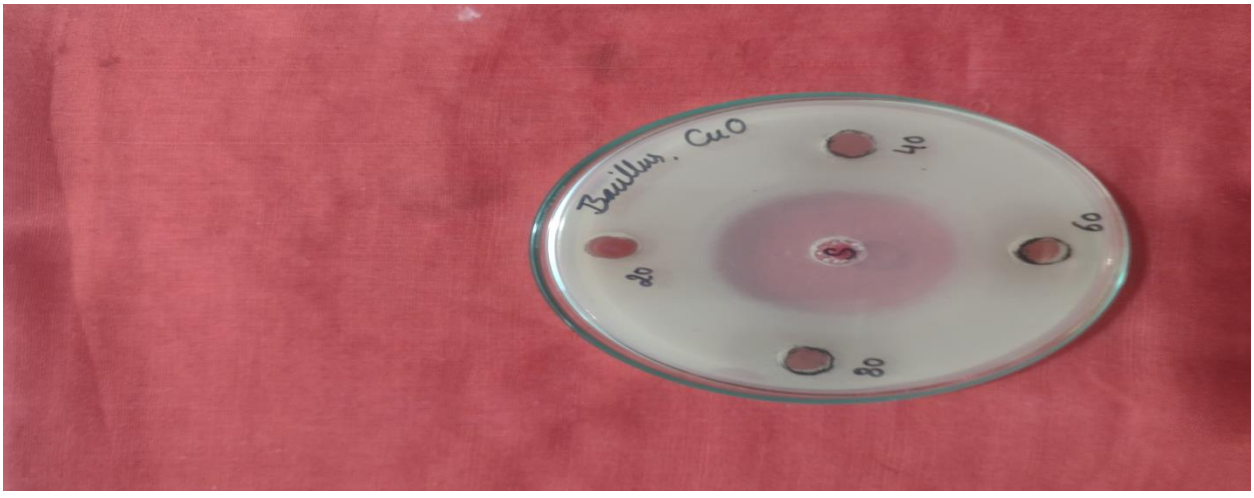

ISSN- 2394-5125 VOL 07, ISSUE 19, 2020

Figure-2

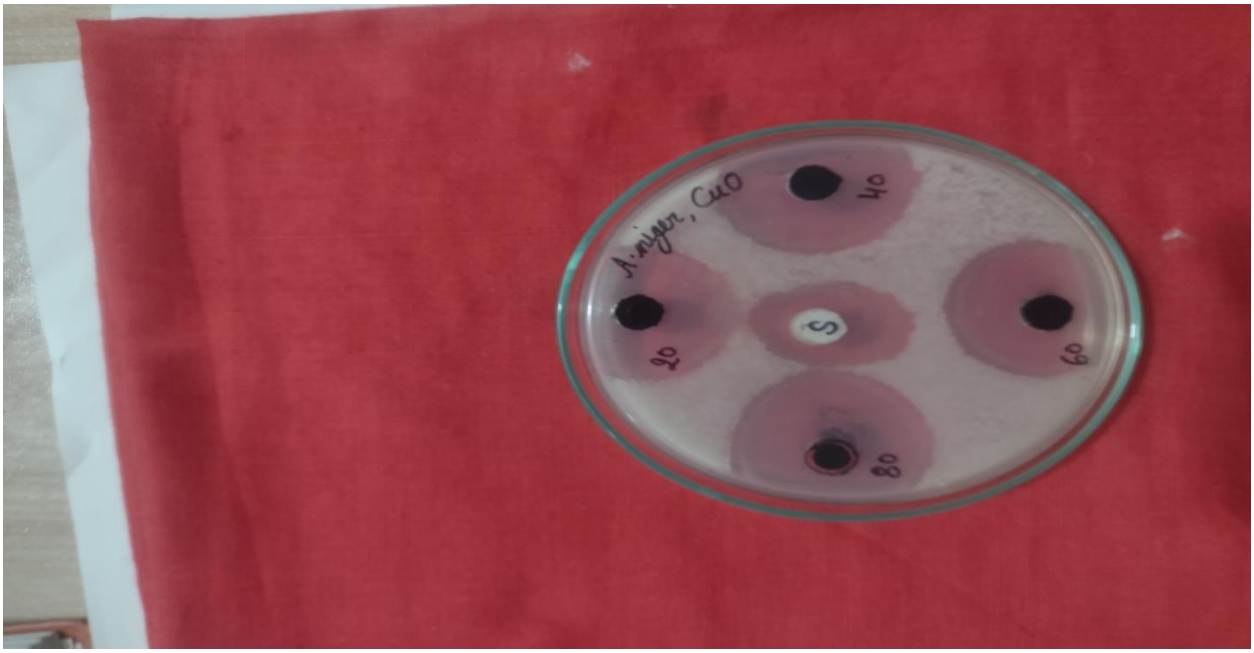


Figure-3

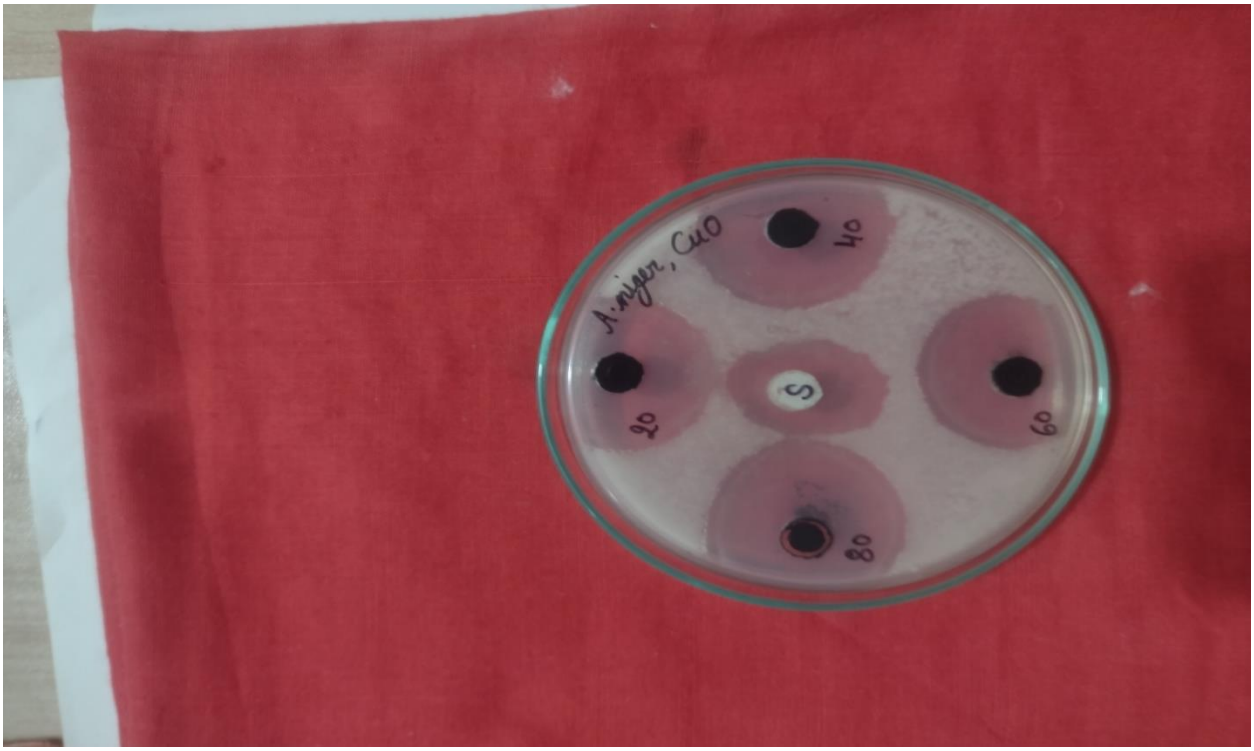


Figure-4

ISSN- 2394-5125 VOL 07, ISSUE 19, 2020

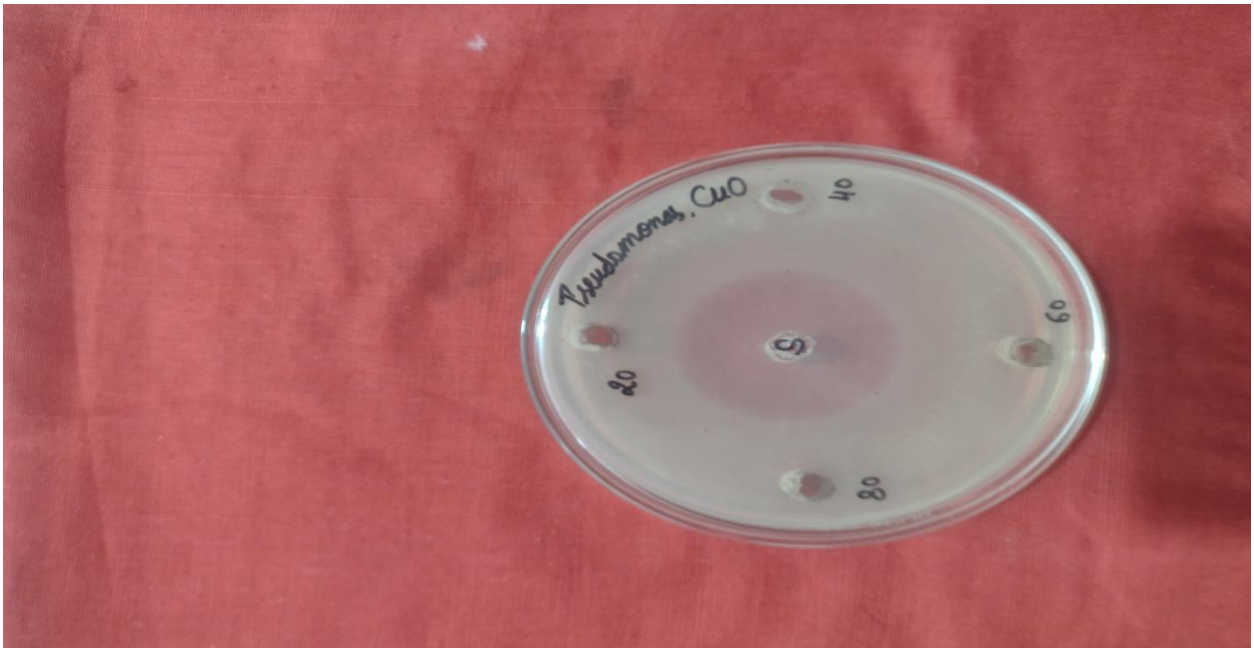


Figure-5

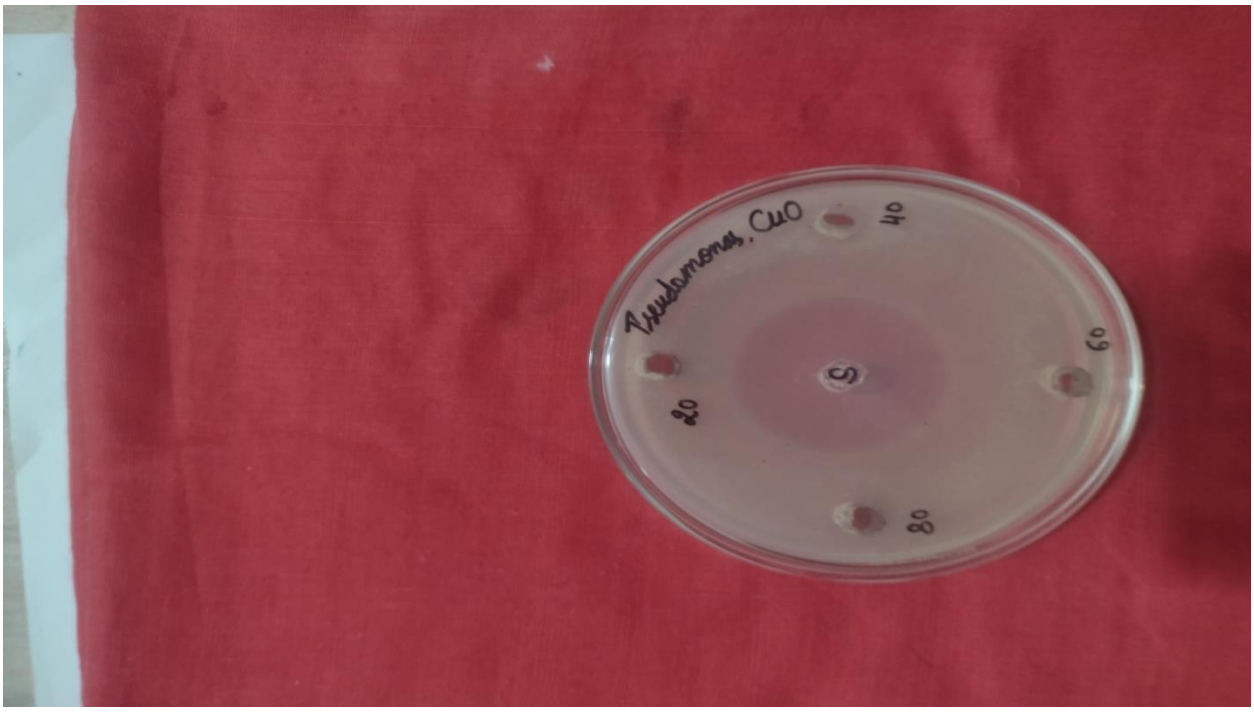


Figure-6

ISSN- 2394-5125 VOL 07, ISSUE 19, 2020

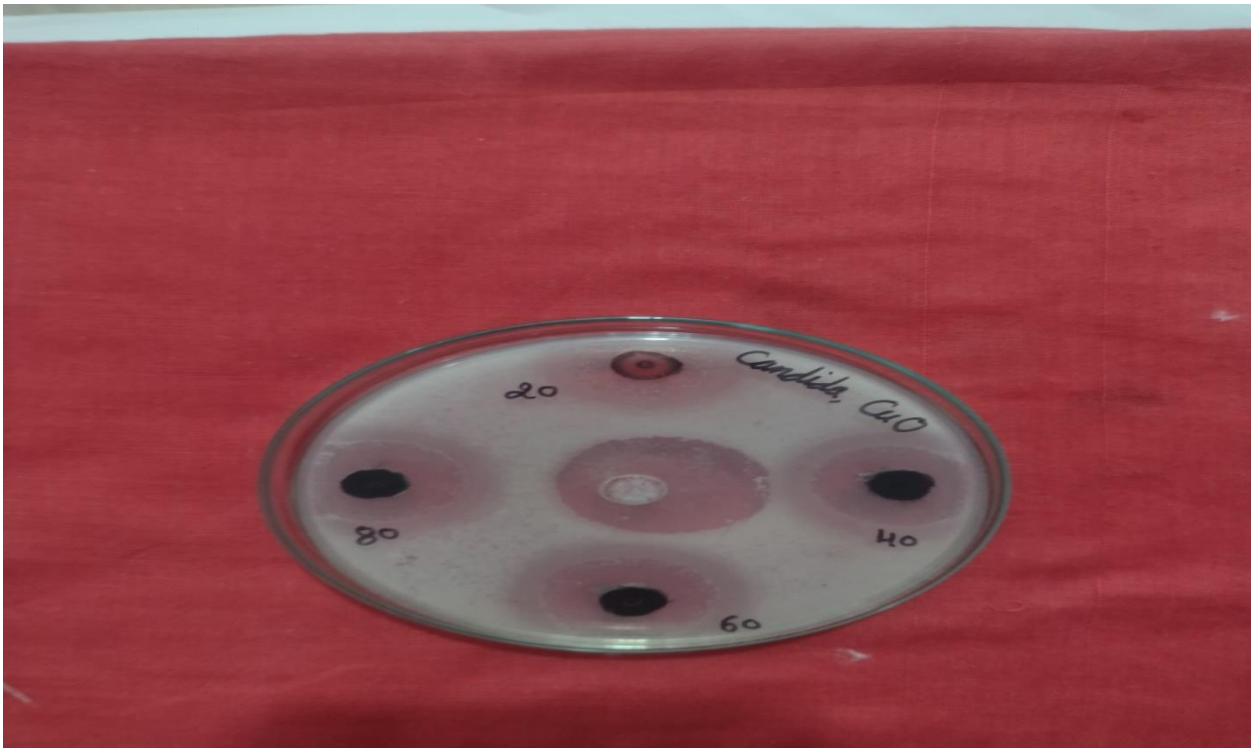


Figure-7

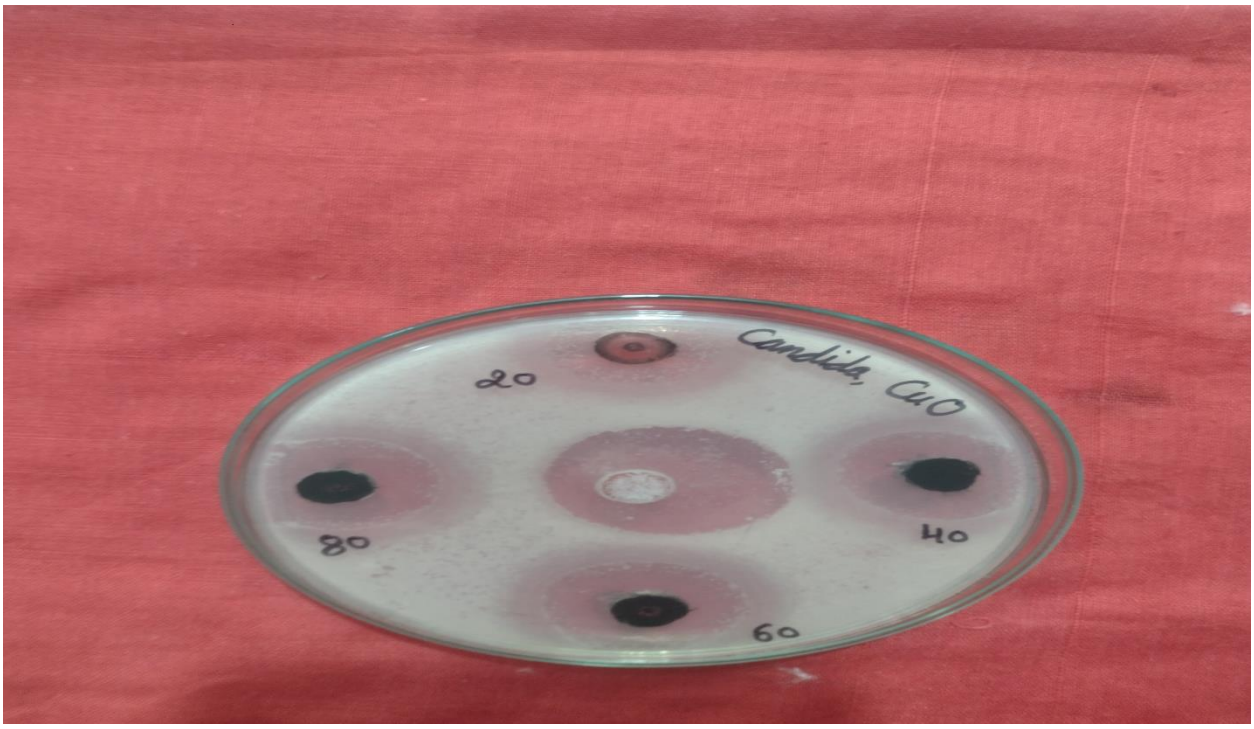


Figure-8

ISSN- 2394-5125 VOL 07, ISSUE 19, 2020

## 14 CONCLUSION

In the current study, the CuO nanoparticles were produced using a wet chemical method using copper nitrate. The CuO nanoparticles had been subjected to testing, and it was discovered that they are anti-bacterial, effective against fungus and bacteria, and can also be used as a contrast agent in ultrasound imaging. The nanoparticles were examined using the fourth probe technique of V-I, XRD, SEM, TEM, FTIR, and UV. In UV analysis, the largest consumption occurs at 2050 nm. Different peaks of beneficial groups from Alcohol/Phenol O-H Stretch, Alkyl C-H Stretch, Aliphatic Esters, and Alkenes are seen in the copper oxide nanoparticles' FTIR spectrum. The study of the SEM and TEM revealed the measurements and particle shape of copper oxide nanoparticles. CuO NPs seem to be crystals according to XRD measurements. The resistivity of the CuO NPs synthesis test came out to be 26.07109. CuO NPs have antibacterial and antifungal properties in biological activity.

In this work, CuO NPs were effectively synthesized and crystallised, and their acoustic properties were suitable for ultrasound imaging. A number of studies showed that adding the NPs to a particular volume had a quantitatively and easily observable influence on improving contrast. as much as is feasible. According to our knowledge, this is the first description of sub-110 to 120 nm particles that are clearly visible in ultrasound. The safety of both of the imaging methods utilised is a key benefit of the recommended NPs over current options.

REFFERENCE-

1. Ren G, Hu D, Cheng EW, Vargas-Reus MA, Reip P, Allaker RP. Characterization of copper oxide nanoparticles for antimicrobial applications. Int J Antimicrob Agents 2009; 33(6): 587-590.
2. Kwak K, Chongyoup K. Viscosity and thermal conductivity of copper oxide nanofluid dispersed in ethylene glycol. Korea-AustRheol j 2005; 17(2): 35-40.
3. Nalwa, H. S. (2000). Handbook of nanostructured materials and nanotechnology. New York: Academic.
4. 2. Alivisatos, A. P. (1996). Semiconductor clusters, nanocrystals, and quantum dots. Science, 271, 933–937
5. Rakhshani, A. E. (1986). Preparation, characteristics and photovoltaic properties of cuprous oxide—a review. Solid State Electronics, 29(1), 7–17.
6. Premkumar, T., &Geckeler, K. E. (2006). NanosizedCuO particles via a supramolecular strategy. Small, 2(5), 616–620.
7. Ren, G., Hu, D., Cheng, E. W., Vargas-Reus, M. A., Reip, P., Allaker, R. P. (2009). Characterization of copper oxide nano particles for antimicrobial applications. International Journal of Antimicrobial Agents, 33(6), 587–590.
8. Zailei, Z., Hongwei, C., Yingli, W., Lianying, S., Ziyi, Z., Fabing, S. (2012). Preparation of hierarchical dandelion-like CuO microspheres with enhanced catalytic performance for dimethyldichlorosilane synthesis. Catalysis Science and Technology, 2, 1953–1960.

ISSN- 2394-5125 VOL 07, ISSUE 19, 2020

9. Taran M.; Rad M.; Alavi M. Antibacterial Activity of Copper Oxide (CuO) Nanoparticles Biosynthesized by Bacillus sp. FU4: Optimization of Experiment Design. Pharm. Sci., 2017, 23, 198-206.
10. JamunaBai A.; RavishankarRai V. Environmental Risk, Human Health, and Toxic Effects of Nanoparticles. Nanomaterials for Environmental Protection, 2014, 523
11. J.G. Bednorz, K.A. Muller, Phys. B 64 (1986) 189–193.
12. A.D. Berry, K.D. Gaskill, R.T. Holm, E.J. Cukauskas, R. Kaplan, R.L. Henry, Appl. Phys. Lett. 52 (1988) 1743–1745.
13. G. Malandrino, G.G. Condorelli, G. Lanza, I.L. Fragala, J. Alloys Compd. 251 (1997) 314–316.
14. G. Malandrino, G.G. Condorelli, G. Lanza, I.L. Fragala, U.S. Uccio, M. Valentino, J. Alloys Compd. 251 (1997) 332–336.
15. A.O. Musa, T. Akomolafe, M.J. Carter, Sol. Energy Mater. Sol. Cells 51 (1998) 305–316.
16. X.G. Zheng, C.N. Xu, Y. Tomokiyo, E. Tanaka, H. Yamada, Y. Soejima, Phys. Rev. Lett. 85 (2000) 5170–5173.
17. T. Ishihara, M. Higuchi, T. Takagi, M. Ito, H. Nishiguchi, T. Takita, J. Mater. Chem. 8 (1998) 2037–2042.
18. T. Ishihara, K. Kometani, M. Hashida, Y. Takita, J. Electrochem. Soc. 138 (1991) 173–176.
19. J. Tamaki, K. Shimanoe, Y. Yamada, Y. Yamamoto, N. Miura, N. Yamazoe, Sens. Actuators, B 49 (1998) 121–125.
20. R.V. Kumar, R. Elgamiel, Y. Diamant, A. Gedanken, J. Norwig, Langmuir 17 (2001) 1406–1410.
21. D. Das, B. Nath, P. Phukon, S. Dolui, Coll Surf. B 101 (2012) 430–433.
22. A. Azam, A.S. Ahmed, M. Oves, M.S. Khan, A. Memic, Int. J. Nanomed. 7 (2012) 3527–3535.
23. CDPR (California Department of Pesticide Regulation) CDPR Database, URL: , 2009a.
24. S. Jammi, S. Sakthivel, L. Rout, T. Mukherjee, S. Mandal, R. Mitra, T. Punniyamurthy, J. Org. Chem. 74 (2009) 1971–1972.
25. K. Zhou, R. Wang, B. Xu, Y. Li, Nanotechnology 17 (2006) 3939–3940.
26. S. Chandrasekaran, Sol. Energy Mat. Sol. C109 (2013) 220–221.
27. J. Ko, S. Kim, J. Hong, J. Ryu, K. Kang, C. Park, Green Chem. 14 (2012) 2391-2393
28. Miller N R, Bamber J C and Meaney P M 2002 Fundamental limitations of noninvasive temperature imaging by means of ultrasound echo strain estimation Ultrasound Med. Biol. **28** 1319–33
29. Katz-Hanani I, Rothstein T, Gaitini D, Gallimidi Z and Azhari H 2014 Age-related ultrasonic properties of breast tissue in vivo Ultrasound Med. Biol. **40** 2265–71
30. Azhari H 2010 Basics of Biomedical Ultrasound for Engineers (Hoboken, NJ: Wiley)
31. Gaitini D, Rothstein T, Gallimidi Z and Azhari H 2013 Feasibility study of contrast-enhanced automated acoustic mammography J. Ultrasound Med. **32** 825–33

ISSN- 2394-5125 VOL 07, ISSUE 19, 2020

32. Klenk C et al 2014 Ionising radiation-free whole-body MRI versus 18f-fluorodeoxyglucose PET/CT scans for children and young adults with cancer: a prospective, non-randomised, single-centre study Lancet Oncol. **15** 275–85
33. Rothstein T, Gaitini D, Gallimidi Z and Azhari H 2010 Investigation of acoustic changes resulting from contrast enhancement in through-transmission ultrasonic imaging Ultrasound Med. Biol. 36 1395–404